Macalester Journal of Physics and Astronomy

Volume 5
Issue 1 *Spring 2017*

Article 9

May 2017

Physical Principles Governing Colloidal Particle Deposition at Low Reynold's Number: Applications to Microbial Biofilms

Sophia Wiedmann
Macalester College, swiedman@macalester.edu

Physical Principles Governing Colloidal Particle Deposition at Low Reynold's Number: Applications to Microbial Biofilms

Abstract

Biofilms formed from the adhesion of microbes to a surface hold great relevance to public health and wastewater management. However, the physical principles underlying the attachment stage of biofilm formation, when individual microbes first come into contact with a substrate, are not well understood. Here I report on a model of colloidal particle attachment to a surface that incorporates the effects of diffusion, advection, gravity, and the hydrodynamic lift and drag forces experienced by polystyrene beads at low Reynold's number. The simulation predicts attachment rates of 1.04x10^(-8)m/s, 0.73x10^(-8)m/s, and 1.29x10^(-8)m/s for beads of radius 0.25 μm, 0.55 μm, and 0.90 μm, respectively. Comparison to experimental data demonstrates that the calculated attachment rates approximate the observed rates, but that they tend to underestimate the experimental observations. The model could be further improved by the addition of other forces influencing particle deposition in a fluid environment.

Cover Page Footnote

This analysis was completed through the REU program at Indiana University funded by the National Science Foundation (NSF PHY-1460882). Thank you to Chris Volz, who designed the simulation as part of his doctoral research, and to Dr. Sima Setayeshgar, who advised my summer research.

I. Introduction

Most microorganisms, such as bacteria and fungi, typically live as single cells inhabiting an aqueous environment. However, under the appropriate environmental conditions, individual cells will attach to a surface and form a heterogeneous cellular aggregate called a biofilm [1] (Fig. 1). The cells within a microbial biofilm are characterized by reduced growth rates, an altered gene expression profile, and the secretion of an extracellular polymeric substance (EPS) matrix that sustains the architecture of the biofilm [1, 2]. The EPS matrix protects the cells from the deleterious effects of the environment, e.g. mechanical disruption or destruction by antibiotics; as a result, biofilms are notoriously difficult and expensive to remove [2, 3]. Microbial biofilms pose significant health concerns when they arise in medical settings, such as on indwelling devices or as the agents of chronic infections [4]. Conversely, biofilms have been highly beneficial in remediating hazardous waste and filtering water supplies [5]. The process by which biofilms develop is multifactorial and not well understood. An active area of research within the field of biofilm development is the study of the initial attachment stage, where single cells come into contact with a substrate. A clearer understanding of how biofilms first form would have important applications to their prevention in medical settings and their promotion for bioremediation.

As microorganisms approach a surface, they experience a variety of physical forces that influence the rate at which they attach to the substrate. Examining the physical principles underlying cellular attachment would elucidate factors that potentially impact biofilm formation. By extension, this could inform the design of technology targeting this process. In this paper, I report on a computational model of biofilm formation that incorporates the effects of diffusion,

advection, settling due to gravity, and hydrodynamic forces that become amplified near the surface. The model simulates the accumulation of colloidal particles, analogous to immotile *Escherichia coli* bacteria, on the bottom surface of a glass chamber within an aqueous environment. A comparison between the numerical results and empirical data on particle deposition published by Chen et al. (2010) demonstrate that the model closely predicts the attachment rate of the colloidal particles under these environmental conditions. However, the model underestimates the actual attachment rates, suggesting that it could be improved by the addition of other physical forces that influence particle behavior prior to surface adhesion.

II. Methodology

Simulation Design

The initial attachment stage of biofilm formation is often modeled experimentally through the use of a parallel plate flow chamber (PPFC) (Fig. 2). Cells or abiotic particles are suspended in a fluid medium and passed through the rectangular chamber of the PPFC. The attachment of particles on the bottom of the chamber over time can then be visualized through a transparent cover and recorded. In order to facilitate comparison between experimental data and the numerical results, our computational model was designed to simulate the conditions within the PPFC for polystyrene particles suspended in water at a concentration of C_0, set to 1 in our model.

A schematic depicting the simulation conditions is given in Figure 3. The rectangular chamber is represented by a two-dimensional slice with a chamber length of 6 cm and a height of 0.0762 cm [6]. The concentration C_0 of beads enters from the left wall, while each of the other

walls is set to a particle concentration of 0. The fluid exhibits a parabolic flow profile down the length of the chamber, given by

$$v_x = v_0 \tfrac{3}{2}(1 - (\eta - 1)^2). \quad (1)$$

Here v_x is the velocity down the length of the chamber, v_0 is the maximum flow velocity, and η is the height y from the bottom surface divided by the chamber half-height $b = 0.0381$ cm. Particle deposition occurs at low Reynold's number, indicating that viscous forces far exceed inertial forces, as would be typical for cells navigating the local fluid environment. Concomitant with a low Reynold's number, only laminar flow is present in the chamber (i.e. there is no turbulence). The simulation assumes that there are no particle-particle interactions and that once a particle comes into contact with the bottom, it permanently attaches.

Governing Equation

The flux of particles on the bottom of the chamber determines the attachment rate. Once the flux has reached its steady state, the attachment rate is given by the magnitude of the flux divided by the inlet concentration C_0. We calculate the flux J as a function of the particle concentration c:

$$\vec{J} = -\boldsymbol{\beta}\nabla c + \vec{v}c \quad . \quad (2)$$

The particles diffuse through the fluid as described by the diffusion coefficient matrix β. This term is determined by the bulk diffusion constant β_0 and two correction factors $\lambda_{\parallel}^{-1}$ and $\lambda_{\perp}^{-1}$ arising from the heightened hydrodynamic drag force experienced by a particle as it nears the surface:

$$\boldsymbol{\beta} = \beta_0 \begin{pmatrix} \lambda_{\parallel}^{-1} & 0 \\ 0 & \lambda_{\perp}^{-1} \end{pmatrix}. \tag{3}$$

For a spherical particle, the bulk diffusion constant is given by $(kT)/(6\pi\mu r)$, where k is the Boltzmann constant, T the temperature, μ the viscosity of water, and r the particle radius. While suspended in the fluid, the particles experience a Stoke's drag force equal to $6\pi\mu r$. Once a particle becomes sufficiently close to the surface, it experiences an increased drag represented by two correction factors [7]. The correction factors that alter the concentration gradient parallel and perpendicular to the surface depend upon the distance h between the surface and the center of a bead of radius r. Generally, the correction factors cannot be written in closed form [8]. The parallel drag correction can instead be approximated as

$$\lambda_{\parallel}^{-1} \approx 1 - \frac{9}{16}\left(\frac{r}{h}\right) + \frac{1}{8}\left(\frac{r}{h}\right)^3 - \frac{45}{256}\left(\frac{r}{h}\right)^4 - \frac{1}{16}\left(\frac{r}{h}\right)^5 . \tag{4}$$

For a spherical object approaching an infinitely large wall (an appropriate approximation for beads of radius around 1μm in a PPFC), the perpendicular drag correction can be written exactly:

$$\lambda_{\perp}^{-1} = \left(\frac{4}{3}sinh\xi \sum_{n=1}^{\infty} \frac{n(n+1)}{(2n-1)(2n+3)} \left(\frac{2sinh\left((2n+1)\xi\right) + (2n+1)sinh\left(2\xi\right)}{4sinh^2\left(\left(n+\frac{1}{2}\right)\xi\right) - (2n+1)^2 sinh^2\left(\xi\right)} - 1\right)\right)^{-1}, \tag{5}$$

where $\xi = cosh^{-1}(h/r)$.

The flux is also a function of the velocity of the particle, v (Eq. 2). The velocity in the $\hat{x}$ direction depends only on advection according to Eq. (1). The component in the direction of $\hat{y}$ results from the effects due to particle settling (gravity) and the hydrodynamic lift and drag forces that become enhanced as the particle approaches the bottom surface.

Gravity acts to augment the attachment rate by increasing the particle velocity towards the bottom of the chamber. The settling velocity due to gravity, v_s, depends on the ratio of the pull of gravity on the effective mass of the particle to the drag it experiences as it moves through the fluid:

$$v_s = \frac{4}{3}\pi r^3 \left(\frac{g(\rho - \rho_{fluid})}{6\pi\mu r} \right) . \quad (7)$$

The specific densities of the polystyrene beads and water are ρ = 1.055 g/cm^3 and ρ_{fluid} = 0.99704 g/cm^3, respectively.

The hydrodynamic lift force F_L tends to push the particle away from the bottom of the chamber as it gets close to the surface. It is determined by the fluid density ρ_{fluid}, the maximum flow velocity v_0, the bead radius r, the half-height of the chamber b, and the function $G(h)$:

$$F_L = \rho_{fluid} r^4 G \left(\frac{v_0}{2b} \right)^2 , \quad (8)$$

$$G = \frac{-5\pi}{12} \left(\frac{h}{b} - 1 \right) \left(73 \left| \frac{h}{b} - 1 \right| - 51 \right) . \quad (9)$$

The lift force and the hydrodynamic drag experienced by the particle both act against the downwards movement of the particle prior to its attachment. Combined with the settling due to gravity, these generate the $\hat{y}$ component of the velocity of the particle:

$$v_y = \lambda_{\perp}^{-1} \left(v_s - \frac{F_L}{6\pi\mu r} \right) . \quad (10)$$

In the simulation, $\lambda_{\perp}^{-1} < 1$.

Delineating the effects of diffusion, advection, settling due to gravity, and the hydrodynamic lift and drag forces allows for the calculation of the particle flux. The attachment

rate can then be computed by dividing the magnitude of the steady-state flux by the inlet concentration, in terms of the nondimensionalized concentration, $\hat{c}$, and height from the bottom, η. The attachment rate just above the surface at a height *dy* is therefore given by

$$AR = \frac{\beta_0 \lambda_\perp^{-1}}{b} \frac{\partial \hat{c}}{\partial \eta}\bigg|_{y=dy} + \lambda_\perp^{-1} \left(v_s - \frac{F_L}{6\pi\mu r} \right) \hat{c}|_{y=dy} \quad . \tag{11}$$

The complete simulation incorporates all the physical effects listed above with a final attachment rate given by Eq. (11). In order to test the accuracy of the model, simpler cases were first considered.

III. Results and Discussion

Smoluchowski-Levich Approximation

The first case only considers the impact of diffusion and advection on the behavior of the beads. This behavior is described by the Smoluchowski-Levich (SL) approximation, which assumes that the repulsive hydrodynamic drag force and attractive van der Waals forces between the particles and the surface cancel [9]. The attachment rate is then solely a function of the change in concentration in the $\hat{y}$ direction:

$$AR = \frac{\beta_0}{b} \frac{\partial \hat{c}}{\partial \eta}\bigg|_{y=dy} \quad . \tag{12}$$

The simulation predictions of particle deposition match the expected behavior based on the analytical solution to Eq. (12). The concentration profiles for various combinations of particle size and flow velocity depict minimal changes in the particle concentration until particles

begin to near the surface (Fig. 4). As the beads permanently attach to the bottom, they are removed from the fluid medium and the bead concentration decreases.

The attachment rates of the SL approximation decrease nonlinearly as a function of bead radius and tend to increase as the flow velocity becomes larger (Fig. 5). The reduction in the attachment rate for larger particles is explained by the inclusion of diffusion in the approximation. Larger particles diffuse less quickly through the fluid.

Smoluchowski-Levich Approximation with Settling

The inclusion of settling due to gravity introduces a second term to the attachment rate that depends on the settling velocity given by Eq. 7:

$$AR = \frac{\beta_0}{b}\frac{\partial \hat{c}}{\partial \eta}\bigg|_{y=dy} + v_s \hat{c}|_{y=dy} \quad . \tag{13}$$

The attachment rates in this scenario exceed those estimated by the SL approximation due to the greater downwards velocity. As a result, the simulation predicts a sharper decrease in bead concentration near the bottom surface (Fig. 6). Initially, the attachment rate decreases for larger bead radii. However, once the radius of the bead has surpassed some critical radius, the attachment rate begins to increase quadratically as the effects of settling dominate over those of diffusion (Fig. 7). The attachment rate tends to increase slightly with the flow velocity.

Smoluchowski-Levich Approximation with Settling and Hydrodynamic Forces

The complete simulation calculates attachment rates according to the formula given in Eq. 11. The hydrodynamic lift and drag forces both oppose the downwards motion due to

diffusion, advection, and settling and will tend to diminish the predicted attachment rates. The attachment rate achieves a minimum at a certain bead radius and then begins to increase in magnitude for larger beads (Fig. 8). The attachment rates are now significantly less than those predicted in the absence of hydrodynamic forces.

The simulation results adhere to the generally expected behavior for the beads as they deposit on the bottom surface. Nevertheless, an important test for the accuracy of the simulation is to confirm that the calculated attachment rates converge as the density of y-grid points increases near the surface.

Simulation Convergence

The simulation was tested for convergence for beads of radius 0.25 μm, 0.55 μm, or 0.90 μm with flow velocities of 0.013 cm/s (the fluid velocity of groundwater) and 0.66 cm/s. The number of y-grid points ranged from 100 to 2000. In each case, the calculated value for the attachment rate begins to converge for large numbers of y-grid points (Fig. 9). Though the simulation exhibits behavior indicative of convergence, it does not appear to reach the maximum value for the attachment rate within the number of y-grid points tested. Due to limited computation time, larger numbers of y-grid points were not able to be tested. However, because the simulation appears to be converging, the correct attachment rate should be able to be calculated either by increasing the number of y-grid points or by extrapolating from the current data. This is required to achieve a better estimate of the attachment rate under the different particle and fluid conditions.

Comparison to Experimental Data

In 2010, Chen et al. published a study examining deposition rates of polystyrene particles in a PPFC. The authors observed attachment rates of $(7.00 \pm 0.40) \times 10^{-9}$ m/s, $(3.34 \pm 0.10) \times 10^{-8}$ m/s, and $(6.36 \pm 0.15) \times 10^{-8}$ m/s for particles of radius 0.25 μm, 0.55 μm, and 0.9 μm, respectively, at a flow velocity of 0.66 cm/s [6]. These values for particle radius and flow velocity were input to the simulation in order to compare the predicted attachment rates to those reported by Chen et al. The simulation calculated attachment rates of 1.04×10^{-8} m/s, 0.73×10^{-8} m/s, and 1.29×10^{-8} m/s for particles of radius 0.25 μm, 0.55 μm, and 0.90 μm, respectively. The numerical results approximate the empirical data, but the calculated attachment rates underestimate those measured experimentally (Fig. 10).

The slow convergence of the simulation could be contributing to this result: though the simulation does begin to converge at large numbers of y-grid points, adding more points would likely lead to an increase in the predicted attachment rates and reduce the difference between the datasets. The underestimation of the attachment rates also suggests that the simulation could be improved by including other forces that might influence particle deposition. For example, cell bodies and polystyrene beads have both been shown to possess a net negative charge in suspension [6], indicating that electrostatic interactions and van der Waals forces between the particles and the surface of the PPFC could impact deposition rates. Further exploration of the roles of these and other forces is required in order to more accurately predict particle attachment.

IV. Conclusion

The simulation discussed here models the deposition of colloidal particles on the bottom surface of a parallel plate flow chamber at low Reynold's number. Polystyrene beads of radius approximately 1μm simulate the behavior of immotile bacteria that are similar in size and form biofilms. The model incorporates the effects of diffusion, advection, gravity, and the heightened hydrodynamic lift and drag forces experienced by the particles as they approach the surface. At a flow velocity of 0.66 cm/s, the simulation predicts attachment rates of 1.04×10^{-8} m/s, 0.73×10^{-8} m/s, and 1.29×10^{-8} m/s for beads of radius 0.25 μm, 0.55 μm, and 0.90 μm, respectively. Comparison to data published by Chen et al. (2010) demonstrates that the simulation provides a good approximation of the experimentally observed attachment rates, but consistently underestimates their magnitude. This is likely due in part to the small number of y-grid points at which the simulation was run. Increasing the number of y-grid points or extrapolating from the results at lower numbers of y-grid points would provide a more accurate estimation of the attachment rates for comparison with data from Chen et al. In addition, this discrepancy could suggest that the accuracy of the model would be improved by the inclusion of additional physical forces affecting particle adhesion, such as electrostatic interactions or van der Waals forces between the particle and the surface. Extending the simulation to greater numbers of y-grid points and further examination of the roles of other forces during particle deposition is required to more accurately assess the validity of the simulation.

References

[1] Donlan, R.M. Emerging Infectious Diseases, **8**, 881 (2002).

[2] Fong, J.N., Yildiz, F.H. Microbiology Spectrum, **3**, doi: 10.1128/microbiolspec.MB-0004-2014 (2015).

[3] Stewart, P.S. Pathogens and Disease, **70**, 212 (2014).

[4] Wu, H., Moser, C., Wang, H.Z., Hoiby, N., Song, Z.J. International Journal of Oral Science, **23**, 1 (2015).

[5] Calderón, K., González-Martínez, A., Gómez-Silván, C., Osorio, F., Rodelas, B., González-López, J. International Journal of Molecular Sciences, **14**, 18572 (2013).

[6] Chen, G., Jong, Y., Walker, S.L. Langmuir, **26**, 314 (2010).

[7] Brenner, H. Advances in Chemical Engineering, **6**, 287 (1966).

[8] Lin, B.H., Yu, J., Rice, S.A. Physical Review E, **62**, 3909 (2000).

[9] Bakker, D.P., Busscher, H.J., van der Mei, H.C. Microbiology, **148**, 597 (2002).

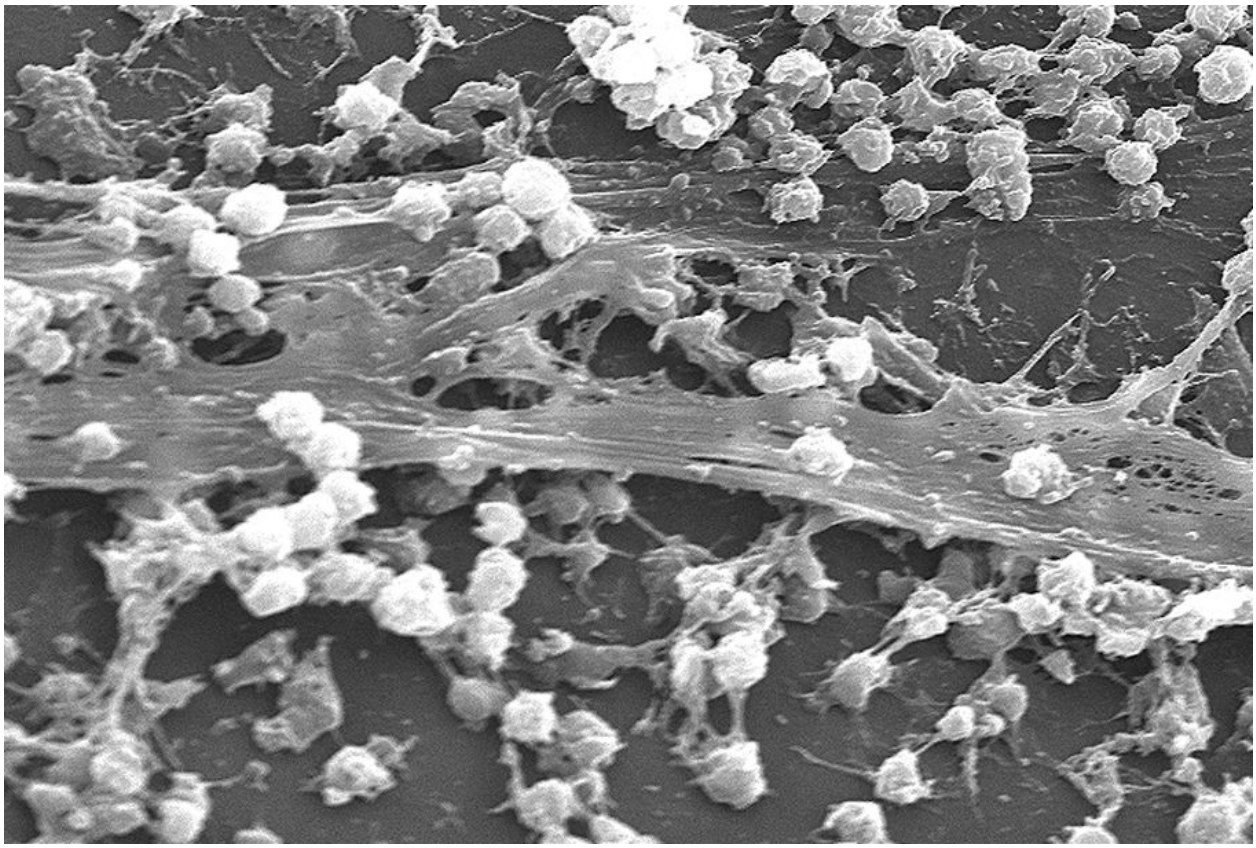

Figure 1. *Staphylococcus aureus* biofilm growing on an indwelling catheter.
An electron scanning micrograph of an *S. aureus* biofilm illustrates characteristic features of biofilms. Bacteria (the round objects) have accumulated and adhered to an indwelling catheter. The cells have secreted an EPS matrix (the web-like material) that stabilizes the biofilm architecture and maintains connections between the bacteria. Magnified 2363x. Image courtesy of CDC Public Health Image Library.

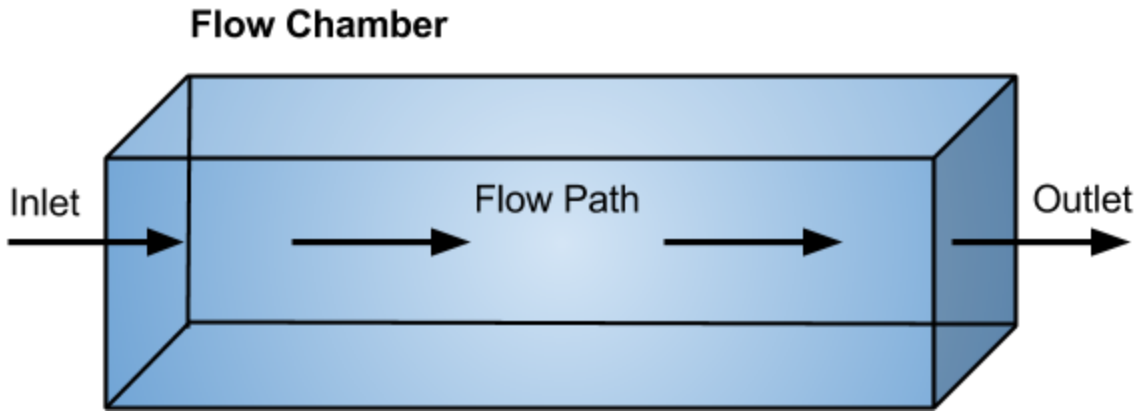

Figure 2. Rectangular chamber of a parallel plate flow chamber (PPFC).
A suspension of particles enters from the left through the inlet, flows through the chamber, and exits through the outlet on the right wall. Particles deposit upon the bottom surface and can be viewed through a transparent coverslip by microscopy.

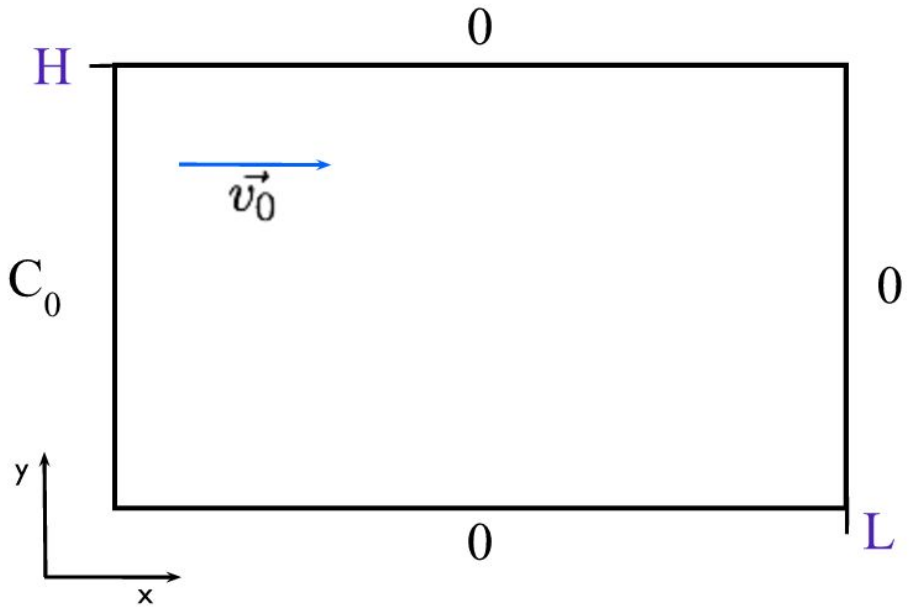

Figure 3. Diagram of simulated flow chamber.
The flow chamber is represented by a rectangular space of height $H = 0.0762$ cm and length $L = 6$ cm. The value of x corresponds to the distance down the length of the chamber, from the inlet to the outlet. The height from the bottom of the chamber is given by y. The left wall represents the inlet and is set to a concentration of C_0. The outlet, top, and bottom are all set to a concentration of 0. The fluid flows to the right with a maximum velocity of v_0 that drops off quadratically on either side, reaching 0 m/s at the walls.

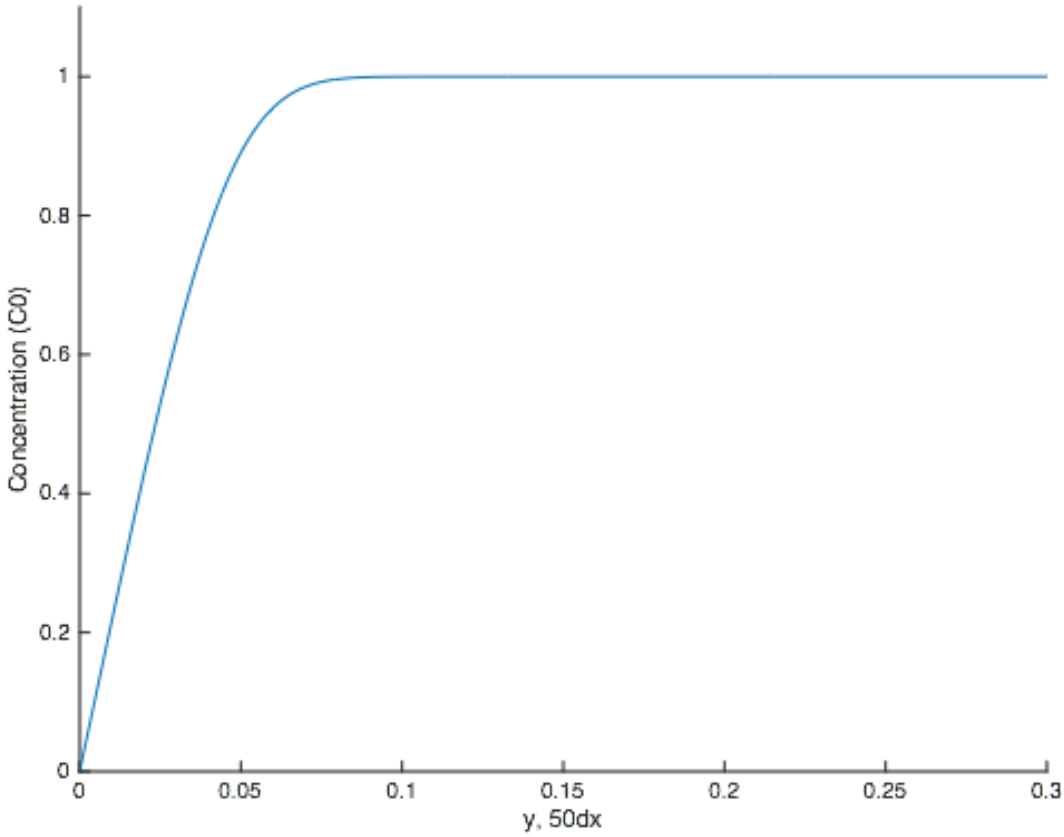

Figure 4. Concentration profile for a 1.0 μm polystyrene bead in a fluid with a flow velocity of 0.1 cm/s (SL approximation).
The concentration profile is determined as a function of *y*, the height from the bottom surface, taken halfway down the length of the flow chamber (50*dx*). The concentration is given relative to the inlet concentration C_0. At $y = 0$ on the bottom of the chamber, the concentration is set to 0.

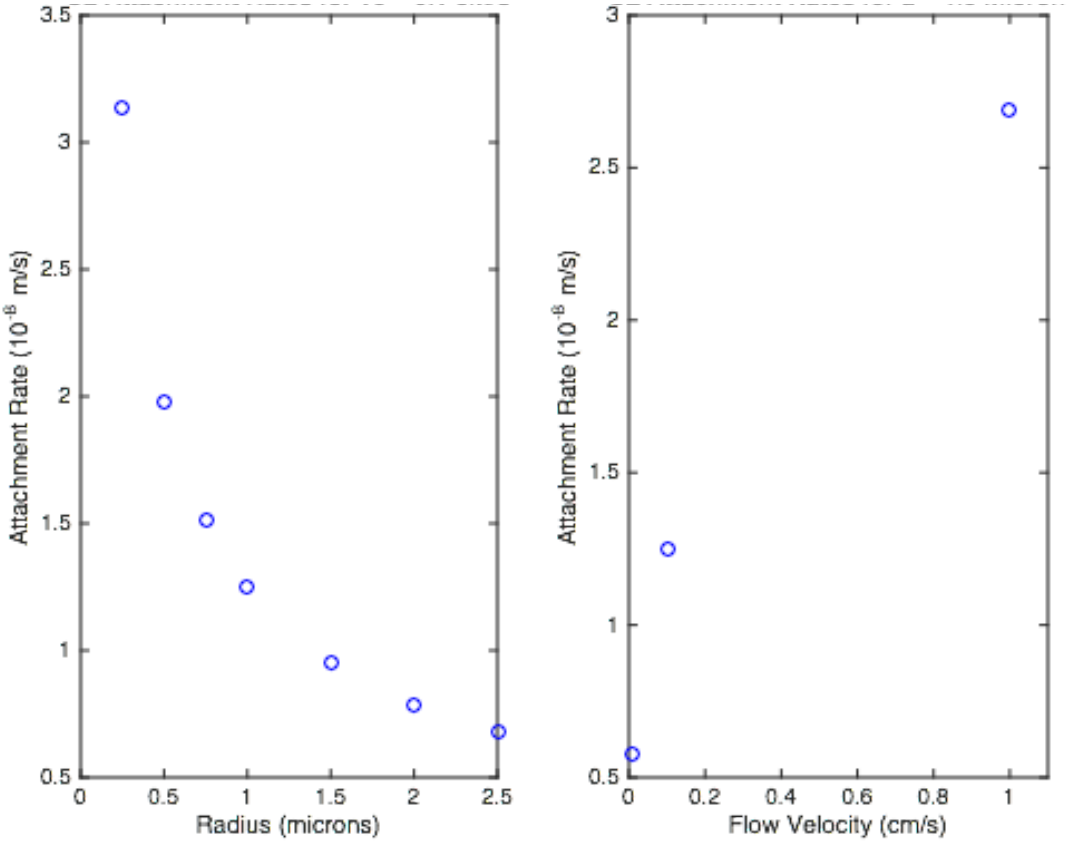

Figure 5. Attachment rates for the Smoluchowski-Levich (SL) approximation.
Left: The attachment rate as a function of particle radius (μm) in a fluid with a flow velocity of 0.1 cm/s. Right: The attachment rates for a particle of radius 1.0 μm experiencing various flow velocities.

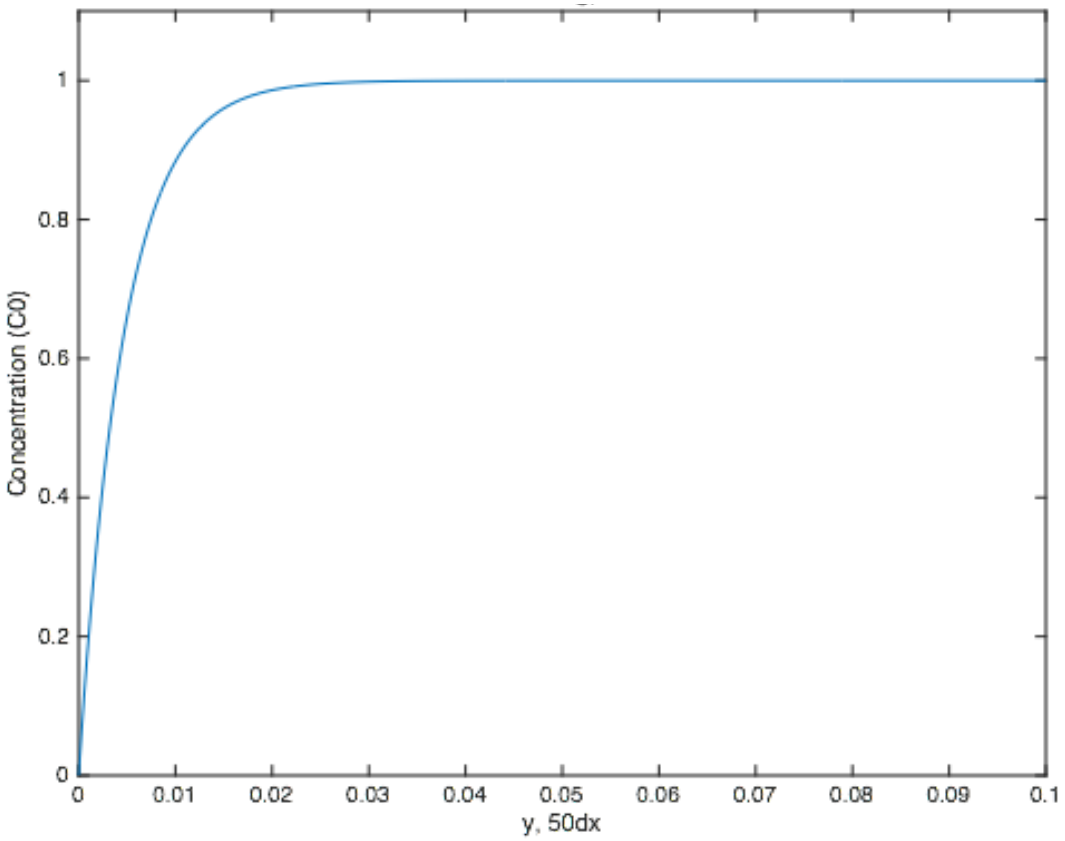

Figure 6. Concentration profile for a 1.0 µm polystyrene bead in a fluid with a flow velocity of 0.1 cm/s (SL approximation with settling).
The concentration profile is a function of *y*, the height from the bottom surface, taken halfway down the length of the flow chamber (50*dx*). The concentration is given relative to the inlet concentration C_0. At $y = 0$ on the bottom of the chamber, the concentration is set to be 0.

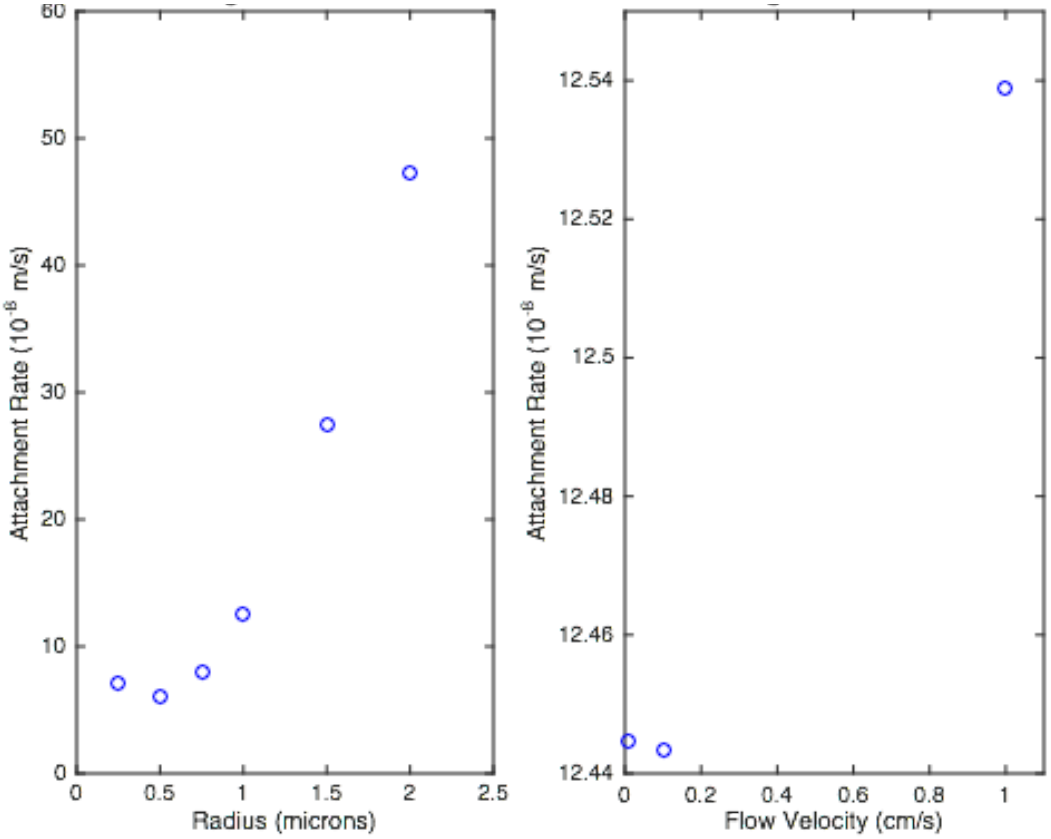

Figure 7. Attachment rates for the the SL approximation with settling.
Left: The attachment rate as a function of particle radius (μm) in a fluid with a flow velocity of 0.1 cm/s. Right: The attachment rates for a particle of radius 1.0 μm experiencing various flow velocities.

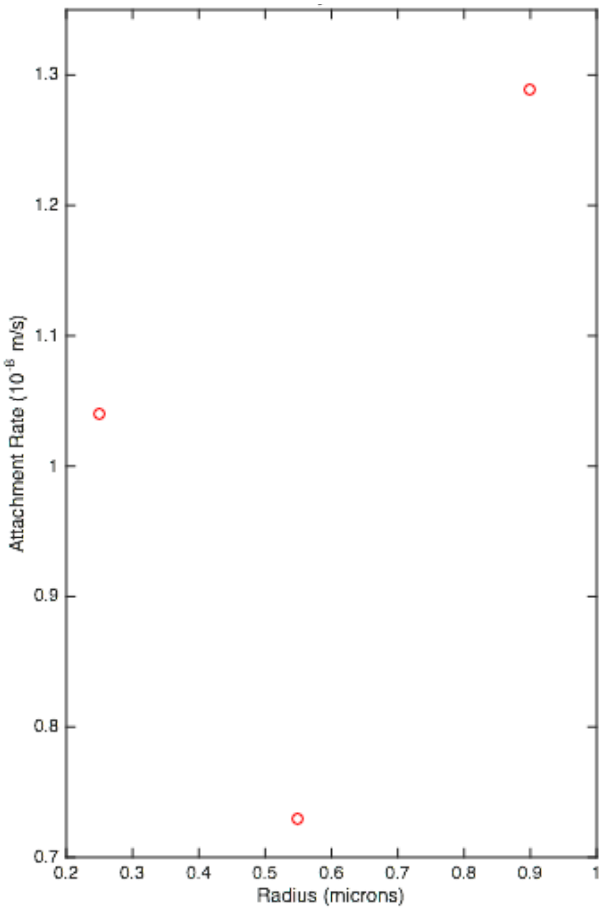

Figure 8. Attachment rates for the the SL approximation with settling and hydrodynamic forces. The attachment rate as a function of particle radius (μm) in a fluid with a flow velocity of 0.66 cm/s. Calculations were performed for the case where the number of y-grid points is equal to 500.

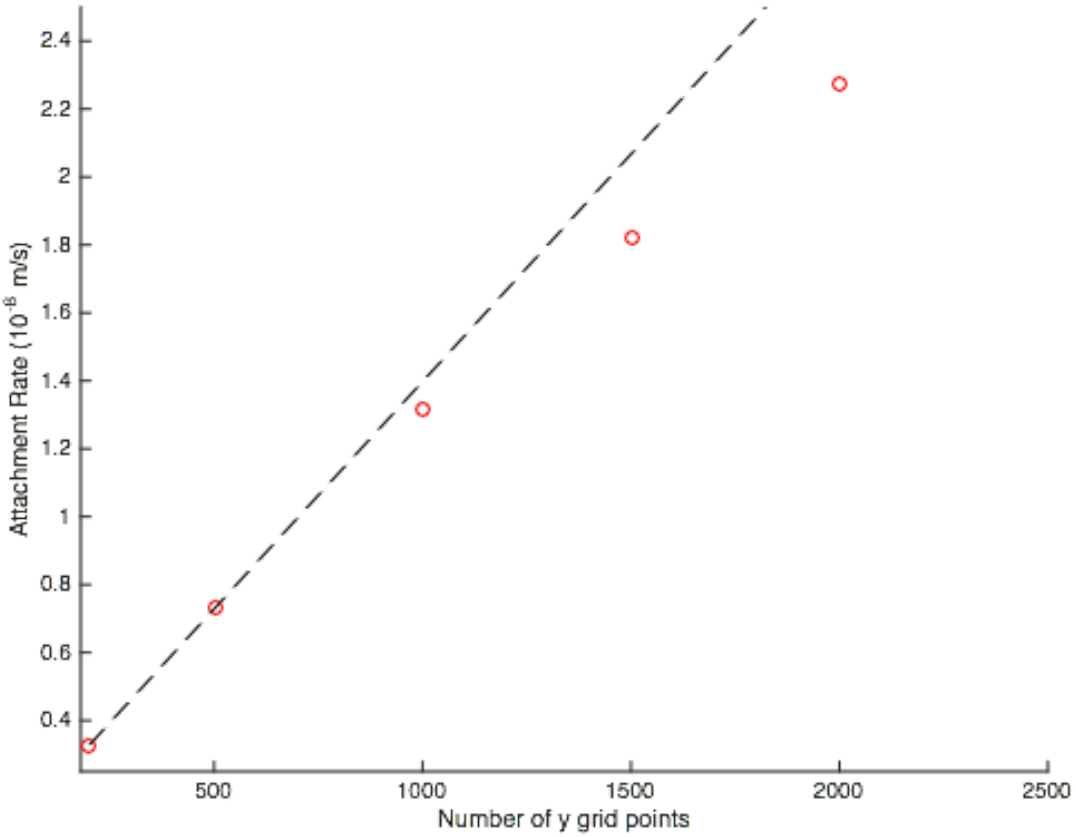

Figure 9. Convergence of the attachment rate for a particle of radius 0.55 μm with a flow velocity of 0.66 cm/s.
The attachment rate for a particle of radius 0.55 μm experiencing a maximum flow velocity of 0.66 cm/s is calculated for a range of y-grid points (red circles). A line connecting the first two points is plotted with the data (dashed line).

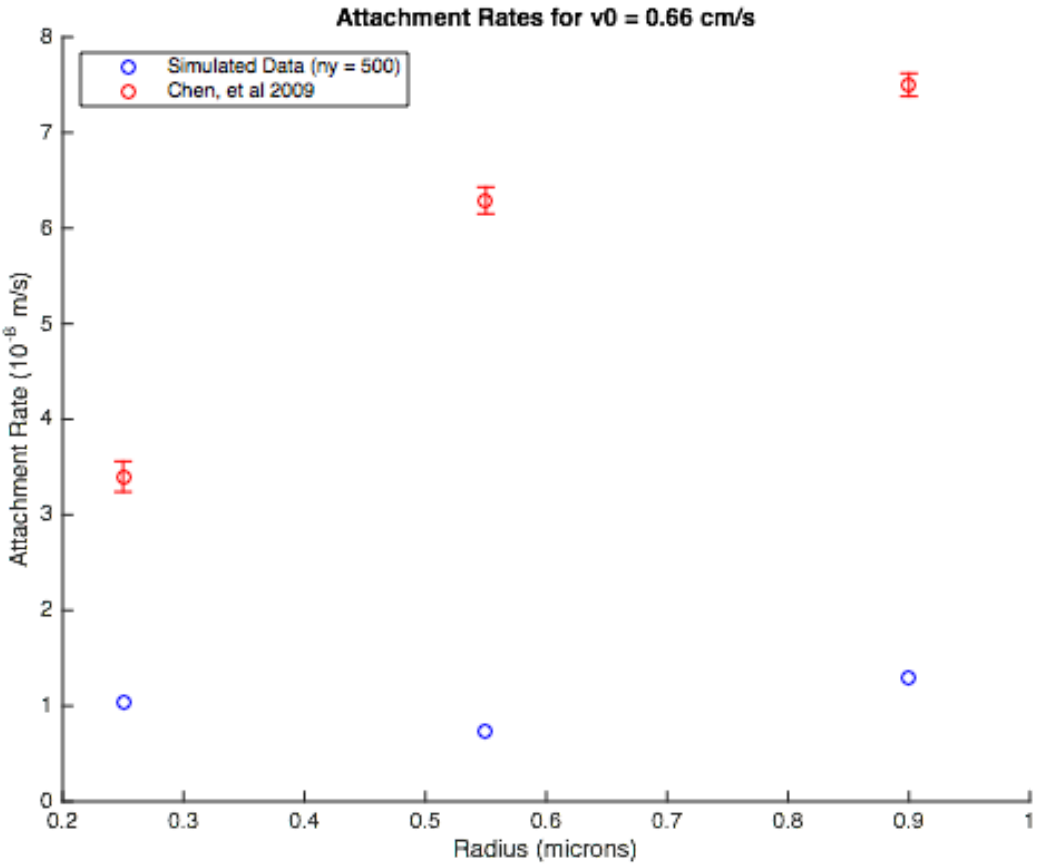

Figure 10. Attachment rates for polystyrene particles in a PPFC with a fluid of velocity 0.66 cm/s.
Chen et al. (2010) reported the attachment rates for polystyrene particles of radius 0.25 μm, 0.55 μm, and 0.90 μm in a fluid of maximum velocity 0.66 cm/s. These data are plotted in red. The simulation output for the same conditions is plotted in blue (number of y-grid points is 500).